Imaging 0.36 nm lattice planes in conjugated polymers by minimizing beam damage

Brooke Kuei,[1] Carol Bator,[2] and Enrique D. Gomez[1,3,4]*

[1]Department of Materials Science and Engineering, The Pennsylvania State University, University Park, Pennsylvania 16802, United States

[2]Huck Life Sciences, The Pennsylvania State University, University Park, Pennsylvania 16802, United States

[3]Department of Chemical Engineering, The Pennsylvania State University, University Park, Pennsylvania 16802, United States

[4]Materials Research Institute, The Pennsylvania State University, University Park, Pennsylvania 16802, United States

*Email: edg12@psu.edu

Keywords: conjugated polymers, transmission electron microscopy, beam damage

TOC graphic:

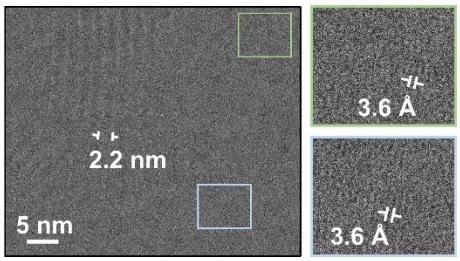

Abstract:

Transmission electron microscopy can resolve the atomic structure of materials with 0.5 Å resolution. High resolution transmission electron microscopy (HRTEM) of soft materials, however, is limited by beam damage. We characterized damage in a series of conjugated polymers comprised of poly(3-hexylthiophene-2,5-diyl) (P3HT), poly(3-dodecylthiophene-2,5-diyl) (P3DDT), and poly[(5,6-difluoro-2,1,3-benzothiadiazol-4,7-diyl)-alt-(3,3’’’-di(2-octyldodecyl)-2,2’;5’,2’’;5’’,2’’’-quaterthiophene-5,5’’’-diyl)] (PffBT4T-2OD) by monitoring the decay of electron diffraction peaks as a function of dose rate, beam blanking, and temperature. We also measured the decay of low-loss electron energy loss spectra as a function of dose rate. These

damage experiments suggest that the dominant mechanism of beam damage in conjugated polymers is the diffusion of a reacting species generated from ionization, likely of side chains. Elucidating a mechanistic description of radiation effects leads to imaging protocols that can minimize damage, which enables the direct imaging of 3.6 Å π-π stacking in a solution-processed conjugated polymer (PffBT4T-2OD), improving state-of-the-art resolution of this class of materials by an order of magnitude.

Introduction

Recent advances in instrumentation have led to transmission electron microscopes with 0.5 Å resolution.[1] High resolution transmission electron microscopy (HRTEM) of soft materials, however, is limited by beam damage.[2-6] The limits of beam damage have been overcome in the structural characterization of proteins through single-particle cryo-EM, which generates reconstructions from hundreds of images of tens of thousands of identical particles present in different orientations.[7-9] For example, the structure of αβ-tubulin was solved with 3.5 Å resolution[10] and protein complexes such as β-galactosidase with an inhibitor were solved at 2.2 Å resolution.[11] This approach has also been employed on nanosheets of a peptoid polymer with ca. 2 Å resolution.[12] Less ordered soft materials, however, cannot be imaged in this way.[4]

Some polymers have been imaged at sub-nanometer resolution using HRTEM, such as through micrographs that reveal defects within poly(p-phenylenebenzobisthiazole) (PBZO) fibers packing at 3.5 Å[13] and images of local variations in crystallite orientation in poly(p-phenylene vinylene) PPV packing at 4.3 Å.[14] While the fully aromatic chemical structure of these polymers makes them more resistant to beam damage,[4, 15-17] the majority of polymers are dominated by C-H bonds that limit their radiation resistance. For example, the application of HRTEM to solution-processable conjugated polymers, which inherently have alkyl side chains, has been limited to the ca. 2 nm lamellar alkyl stacking corresponding to the (100) reflection. HRTEM of poly(3-hexylthiophene-2,5-diyl) (P3HT) reveals how P3HT crystals are ordered within fibrils.[18] Recent studies have also imaged highly ordered lamellar nanostructures and overlapping domains of poly([N,N'-bis(2-octyldodecyl)-naphthalene-1,4,5,8-bis(dicarboximide)-2,6-diyl]-alt-5,5'-(2,2'-bithiophene)) (PNDI2OD-T2),[19] as well as the effect of alkyl side chains on intercrystallite ordering in poly(benzo[1,2-b:4,5-b′]dithiophene−thieno[3,4-c]pyrrole- 4,6-dione) (PBDTTPD).[20]

Nevertheless, the extent of connectivity of π-π stacked regions, which is important for charge transport,[21-25] is not resolvable.

Despite the significant progress that TEM has enabled by resolving the ca. 2 nm (100) spacings of solution-processable conjugated polymers, imaging the ca. 4 Å π-π spacing corresponding to the (010) reflection remains a challenge. This limitation, which has prevented the study of a key pathway for charge transport, is due to the inherently low contrast and beam sensitivity of soft materials. Contrast and sensitivity to the beam are related because the latter limits the number of electrons that can be used for imaging. The number of electrons Q incident on an area d^2 will be $Q = Jd^2$, where d is the smallest resolvable feature size and J is the electron dose. The contrast between domains must be greater than the noise, which is $\sqrt{Q}/Q$ or, equivalently, $1/\sqrt{Jd^2}$.[2, 26] As such, the low contrast often found in soft materials under the TEM and sensitivity to the electron beam limits imaging resolution.

Although the primary processes of radiation damage in soft materials are known to be ionization and excitation, the secondary processes that follow are complex and, consequently, the effects of damage at different imaging conditions is not well understood.[17, 27-29] Electron energy-loss spectroscopy (EELS) damage experiments using the 7 eV π-π* peak of polystyrene, for example, revealed that π bonding is more stable at high dose rates, which was rationalized by the idea that damage occurs via fast secondary electrons that cause damage outside the area illuminated by the beam.[30] EELS experiments on thin films of collodion, however, first show an increase and then a decrease in stability with increasing dose rate. This was attributed to diffusion-limited damage at lower dose rates and local heating from the beam at higher dose rates.[31] Conversely, a more recent diffraction damage study of a polymer/fullerene blend suggests that there is no dose rate dependence on beam damage.[32] Beam damage studies of derivatives of polydiacetylene

suggest that damage occurs through cross linking.[33] In synchrotron X-ray scattering experiments, it has been suggested that protein crystals are damaged through the diffusive motion of radicals and groups of atoms.[34] Because beam damage limits the achievable resolution in HRTEM of soft materials, it is important to elucidate the key factors that govern damage mechanisms, to then develop approaches for minimizing damage.

In this work, we use a systematic study of conjugated polymers to examine the mechanism for beam damage. The use of conjugated polymers allows us to study beam damage effects on both the crystal structure and chemical structure. We calculate critical dose from the decay of diffraction peaks (damage to crystals) as a function of dose rate, temperature, and beam blanking. We also calculate the critical dose for damage from the decay of low loss electron energy loss spectroscopy peaks (bonds breaking) as a function of dose rate. Our results show that damage occurs through the diffusion of a reacting species generated by exposure to the beam; we hypothesize that ionization of side chains is the main culprit. This insight suggests conditions most suitable for imaging beam-sensitive materials, and we successfully use these conditions to directly image the 3.6 Å π-π stacking in a solution-processed conjugated polymer.

Materials and Methods

TEM sample preparation: For diffraction experiments, 10 mg/mL solutions of PffBT4T-2OD (8.8 kg/mol, Đ of 1.068, Solarmer), P3HT (50.9 kg/mol, Đ of 2.23, 96% H-T regioregularity, Merck), and P3DDT (60.0 kg/mol, regioregular, Sigma-Aldrich) were made with chlorobenzene (Sigma-Aldrich) in a nitrogen glove box and stirred for a minimum of 10 hours at 45°C. For imaging experiments, the concentration was reduced to 3 mg/mL to avoid overlapping crystals. Silicon wafers were cleaned through sonication for 20 minutes in acetone and 20 minutes in isopropanol

followed by 15 minutes of ultraviolet light ozonation. PEDOT:PSS (Clevios P, H.C. Starck) was spin-coated onto the silicon wafers in air, after which the polymer of interest was spin-coated onto the PEDOT:PSS film inside a nitrogen glove box. Films were floated off in deionized water and then picked up with copper TEM grids. Samples were dried overnight at room temperature under vacuum and then annealed in a nitrogen glove box. P3HT samples were annealed at 165°C for 3 hours and P3DDT and PffBT4T-2OD samples were annealed at 130°C for 1 hour. Diffraction samples are ca. 90 nm and imaging samples are ca. 30 nm thick.

Critical dose diffraction experiments: Diffraction experiments were carried out on the FEI Tecnai G20 XTWIN at the Penn State Materials Characterization Lab operating at 200 kV with a Gatan UltraScan CCD. Dose rate was determined using the fluorescent screen current, which was in agreement with counts measured at the camera with Digital Micrograph provided that the beam is spread larger than the fluorescent screen (**Figure S1**). Dose rates were measured in areas of vacuum in the sample, after which a selected area aperture and beam stop were inserted and diffraction patterns were collected on the sample with 1s exposure times at 3s intervals using the Digital Micrograph Acquire Series plug-in. A camera length of 330 mm was used. For cryogenic experiments (ca. 93 K), a Gatan 626 Cryo TEM holder was used. 300kV diffraction experiments at cryogenic conditions (ca. 83 K) were carried out on the Titan Krios at the Penn State Materials Characterization Lab with a Falcon 3ec direct electron detector. Diffraction patterns were collected manually using a timer.

Critical dose electron energy-loss spectroscopy (EELS) experiments: EELS experiments were carried out on the TEAM 0.5 at the National Center for Electron Microscopy, Lawrence Berkeley

National Laboratory operating at 80 kV in diffraction mode. 80kV is used because scattering cross section scales linearly with the inverse of the accelerating voltage; thus, low-loss signal is more apparent at 80kV than at higher accelerating voltages. The microscope was equipped with a gun monochromator resulting in ~0.1-0.15 eV energy resolution. A GIF Tridiem filter was used with a 2.5mm aperture. A screen current of around 1 nA was used and beam size was varied to change dose rate. Times series of low-loss EELS peaks were acquired using PEELS View in TIA.

High-resolution TEM: High-resolution imaging experiments were conducted on the Titan Krios at the Penn State Materials Characterization Lab operating at 300kV with a Falcon 3ec direct electron detector in counted mode (without dose fractionation due to a short exposure time, unless otherwise noted). Dose rate was measured with EPU software using the direct electron detector. Grids with experimental samples were cooled to liquid nitrogen temperature (ca. 83 K) inside the autoloader. The microscope was operated in nanoprobe mode with a spot size of 5 and an illuminated area of 0.65 μm at a magnification of 470,000x. We used a dose rate of 75 e/Å^{2}s and an exposure time of 1.07s (unless otherwise noted). We used an applied defocus of -1.00 μm. No camera pixel binning was used (binning of 1).

Results

We quantitatively characterize beam damage in a series of conjugated polymers (chemical structures shown in **Figure 1a**) by calculating critical dose (D_C) values from the decay of electron diffraction peaks. This is done by collecting a series of electron diffraction patterns at a predetermined dose rate. As show in **Figure 1b**, the π-π diffraction ring fades away as dose is accumulated and the crystal structure is damaged. Each diffraction pattern is azimuthally

integrated (**Figure 1c**) and the background subtracted intensity of the π-π peak is plotted as a function of accumulated dose (**Figure 1d**), revealing an exponential decay. D_C, which is defined as the electron dose at which the intensity drops to $1/e$ of its initial value, can then be calculated by taking the inverse of the decay rate, as described by equation 1

$$I = A \exp\left(-\frac{D}{D_c}\right) + I_b \qquad (1)$$

where I is the diffraction peak intensity, A is an exponential prefactor, D is the accumulated dose, and I_b is the background intensity. A higher critical dose therefore corresponds to increased stability under the electron beam.

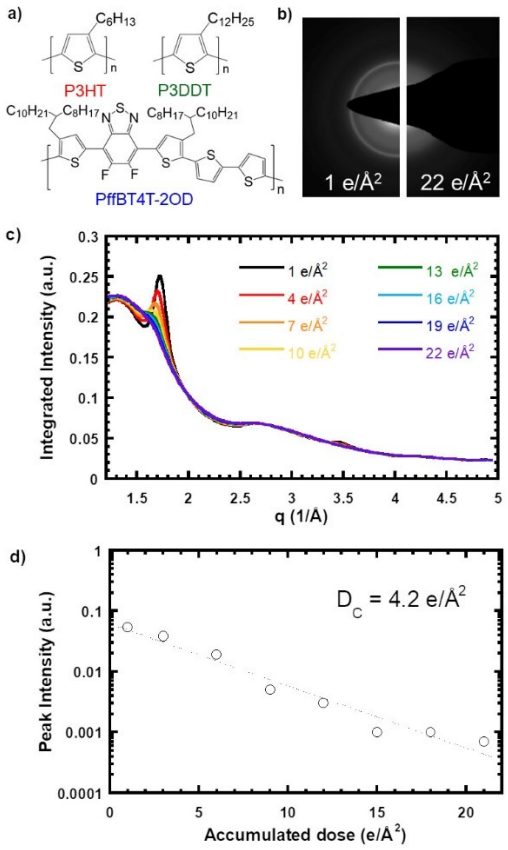

Figure 1. Example of critical dose (D_C) calculation (using PffBT4T-2OD at 1 e/Å^{2}s). (a) Chemical structures of polymers used in this study. (b) Electron diffraction patterns at low and high electron dose, showing loss of diffraction ring (damage of crystal structure) caused by continuous exposure to the electron beam. (c) Azimuthally-integrated electron diffraction corresponding to various accumulated doses, showing a decrease in diffraction peaks with increasing electron dose. (d) Peak intensity (background subtracted, not normalized) plotted against accumulated dose showing exponential decay and fit.

We calculated the critical dose for poly(3-hexylthiophene-2,5-diyl) (P3HT), poly(3-dodecylthiophene-2,5-diyl) (P3DDT), and poly[(5,6-difluoro-2,1,3-benzothiadiazol-4,7-diyl)-alt-(3,3’’’-di(2-octyldodecyl)-2,2’;5’,2’’;5’’,2’’’-quaterthiophene-5,5’’’-diyl)] (PffBT4T-2OD). We characterized damage as a function of dose rate in the dose rate range of 1 e/Å^{2}s to 10 e/Å^{2}s at room temperature (**Figure 2**) and observe that critical dose increases with increasing dose rate. Across the full dose rate range, we also see that critical dose decreases as we go to longer and more

branched side chains. Although the dose rate is often not reported, we note that our values for D_C are consistent with previous results (D_C for P3HT of 16 – 32 e/Å^2).[35, 36]

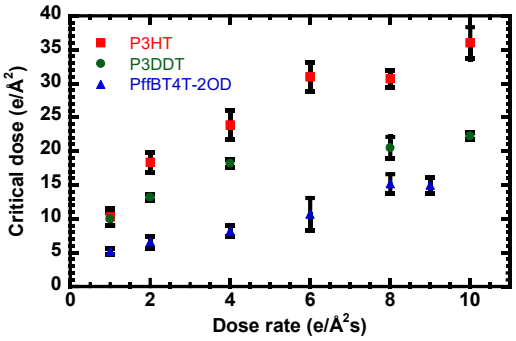

Figure 2. Critical dose for beam damage at room temperature as a function of dose rate for P3HT, P3DDT, and PffBT4T-2OD at 200kV. Critical dose increases with increasing dose rate. Overall, critical dose decreases for polymers with longer and more branched side chains.

We also investigated the effect of beam blanking on the critical dose of P3HT at 1 e/Å^{2}s at room temperature (**Figure 3**). When the beam is not blanked, as in the previous set of experiments, the sample is exposed to the beam throughout the entire acquisition of diffraction patterns, even when an exposure is not taking place. During the beam blanking experiment, the beam is blanked in between exposures (**Figure 3a**). We observe that beam blanking reduces the critical dose, similar to reducing the dose rate. Blanking for longer periods of time results in increasingly lower critical doses. This experiment demonstrates that damage is happening even in the absence of irradiation.

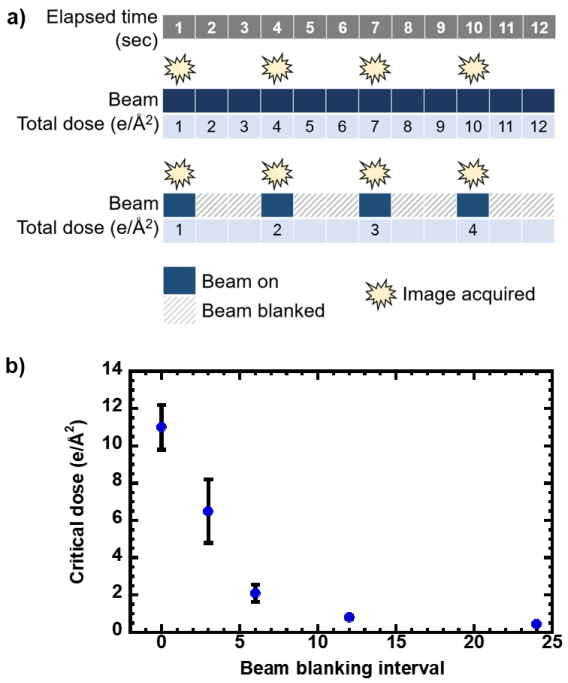

Figure 3. Beam blanking experiments of P3HT at 1 e/Å^{2}s at 200kV. (a) Schematic depicting experimental set-up. Without beam blanking, the sample is exposed to the beam throughout the entire series of diffraction patterns. With beam blanking, the beam is blanked between exposures. (b) The critical dose decreases with beam blanking, and blanking for longer periods of time results in increasingly lower critical doses.

We also calculated the critical dose of P3HT, P3DDT, and PffBT4T-2OD at cryogenic conditions at a dose rate of 1 e/Å^{2}s. For all three polymers, the critical dose increases almost an order of magnitude from room temperature to cryogenic conditions (**Figure 4a**). At cryogenic conditions, the three polymers roughly have the same critical dose (differences in critical dose between polymers are less pronounced than at room temperature). We also calculate the critical dose for PffBT4T-2OD at cryogenic conditions at a range of dose rates (**Figure 4b**) at both 200kV and 300kV. We find that the dose rate dependence that was observed at room temperature is no longer seen and that the effect of accelerating voltage is negligible under cryogenic temperatures.

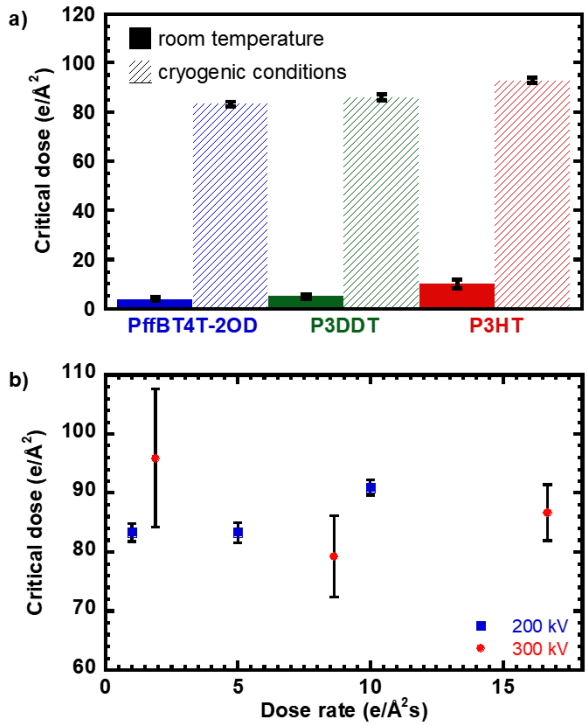

Figure 4. Beam damage at cryogenic conditions. (a) Critical doses of PffBT4T-2OD, P3DDT, and P3HT at 1 e/Å^{2}s at room temperature and cryogenic conditions at 200kV. At cryogenic conditions, the critical dose increases almost an order of magnitude. (b) Critical dose of PffBT4T-2OD at cryogenic conditions as a function of dose rate. At cryogenic conditions, the dose rate dependence is not as prevalent as at room temperature and critical dose at 200kV and 300kV are similar.

An advantage of characterizing damage in conjugated polymers is that in addition to measuring damage with diffraction, we can also measure damage using electron energy-loss spectroscopy (EELS). Here, our low loss signal comes from the electronic structure of the conjugated polymer and can be used to track damage to chemical bonds (**Figure S2a**). We observe the same trend as in diffraction experiments: critical dose increases with increasing dose rate (**Figure S2b**).

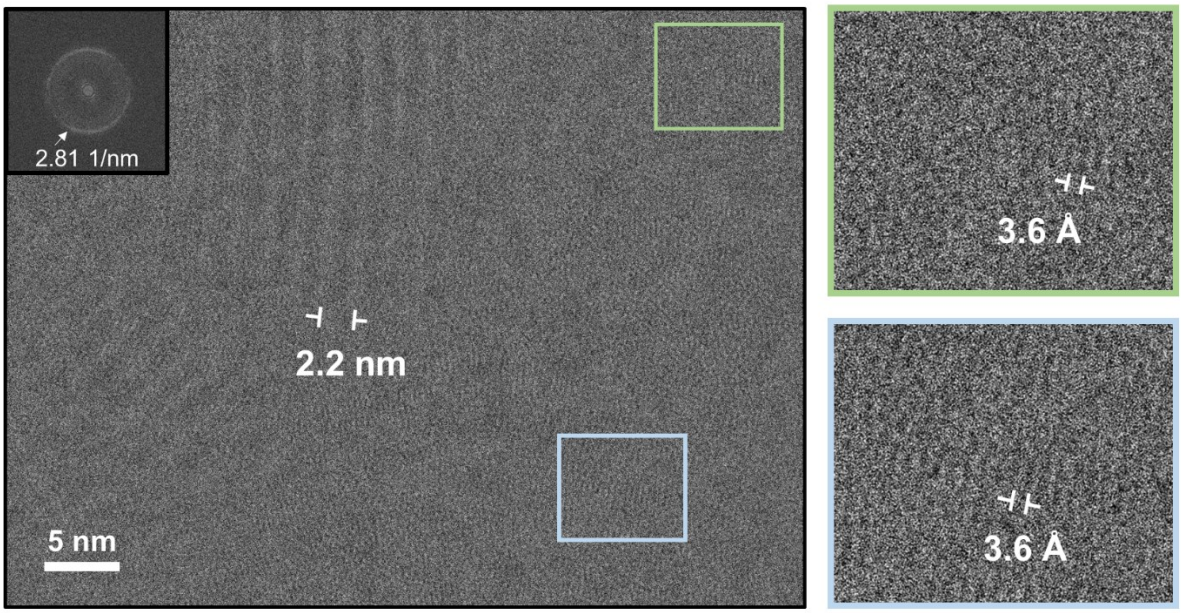

Figure 5. HRTEM of PffBT4T-2OD showing a region with both 2.2 nm (100) lattice fringes and 3.6 Å π-π stacking. FFT in inset shows arcs at 2.81 1/nm corresponding to the π-π stacking. Green and blue insets show magnified π-π stacks.

The advent of new instrumentation and software, particularly those intended for biological samples, offers new opportunities for imaging of polymers. Here, we take advantage of a direct electron detector and automated acquisition software and combine them with new insights from our beam damage experiments. Our critical dose experiments suggest that the highest resolution can be achieved in solution processed conjugated polymers using cryogenic conditions with a critical dose of approximately 80 e/Å^2. The trend with respect to dose rate also suggests that damage can be outrun as higher dose rates are achieved (Figure 2), although not under cryogenic conditions (Figure 4b). Thus, using a total dose of ~80 e/Å^2 at cryogenic conditions, we directly image the 3.6 Å π-π stacking of PffBT4T-2OD in real space. **Figure 5** shows a representative HRTEM image of PffBT4T-2OD taken at minimized damage conditions (additional examples are shown in **Figure S3** and **Figure S4**). We can see the larger (100) spacings that are 2.2 nm. We can also see π-π stacking, both in the real space image and in the Fast Fourier transform (FFT), with a

distance of 3.6 Å, in agreement with X-ray scattering (**Figure S5**).[37, 38] This demonstration of direct imaging of π-π stacking in a solution processed conjugated polymer was made feasible by systematic damage experiments. We observe that the π stacks are longer than they are wide and form a network for charge transport throughout the entire field of view. This is consistent with recent maps of the diffraction of π stacked domains generated with a 2 nm probe.[39] The π stacks, which represent edge-on domains, also appear to overlap with face-on domains.

Discussion

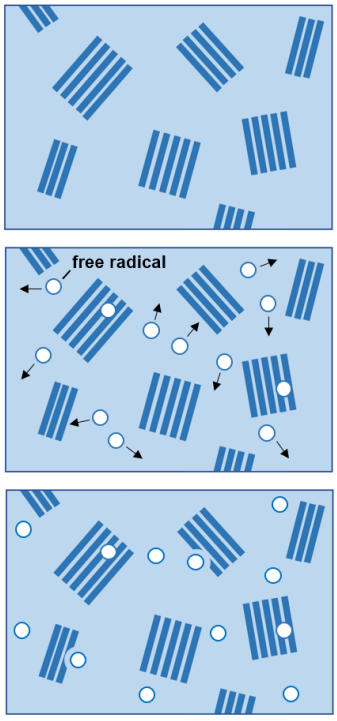

Figure 6. Schematic of beam damage in conjugated polymers. Dark blue regions represent crystalline domains and light blue regions represent amorphous areas. Exposure to the electron beam generates a free radical reacting species in the conjugated polymer (likely from side chain scission) that then diffuse around, causing further damage to the material.

Altogether, our beam damage experiments reveal that at room temperature the critical dose increases with increasing dose rate and decreases with longer side chains; we also found that

damage is worse with beam blanking in between exposures. At cryogenic conditions, we found that the critical dose increases by almost an order of magnitude compared to room temperature. To explain these trends, we propose that damage occurs through the diffusion of a reacting species that is generated by ionization of the side chains. Indeed, recent work shows that blending PffBT4T-2OD, P3HT, or P3DDT with ca. 10 wt% of free radical scavengers, such as butylated hydroxytoluene, leads to an increase in D_C by a factor of about three.[40] As the reacting species diffuses around, it causes further damage to the material in a cascading manner (**Figure 6**). The radicals are likely coming from side chains because aromaticity, such as that in the polymer backbones, imparts radiation resistance to polymers due to delocalized resonance.[4, 16, 17, 41, 42] It is likely like the radical being formed is an alkyl radical, as this is the radical most commonly produced during irradiation of linear polymers such as polyethylene.[43, 44]

At low dose rates, the reacting species has time to diffuse around and cause damage, resulting in a lower critical dose. As we move to higher dose rates, critical dose increases because this diffusion process is outrun. P3DDT is more easily damaged than P3HT because it has a higher ratio of alkanes to aromatics, resulting in a higher population of reacting species. PffBT4T-2OD is most easily damaged perhaps because of its branched side chains. Branched alkanes can undergo rapid primary rearrangement processes that make recombination at bond scission sites unlikely.[17] Also, branched side chains will generate more secondary and tertiary carbocations, which are more stable and likely to diffuse further distances and cause more damage than primary carbocations forming in linear side chains of P3HT and P3DDT. At cryogenic conditions, the critical dose increases overall and the dose rate dependence becomes less pronounced because the low temperature suppresses diffusion of reacting species. Also, because radiolysis is more significant as accelerating voltage is decreased, the observation that different accelerating voltages appear to

cause similar damage at cryogenic conditions suggests that the amount of radiolytic products created matters less than the damage caused by their diffusion.

Cross linking of alkyl side chains is a possibility; we also speculate that significant amounts of reacting species are generated. As such, the diffusion of these reacting species is likely the dominant damage mechanism in conjugated polymers, as has been previously speculated.[45] This is supported by our beam blanking critical dose experiments, in which damage is worse when the beam is blanked and unblanked throughout the duration of the damage experiment. This suggests that damage (through the diffusion of a reacting species) is occurring even when the sample is not illuminated by the beam. Our observation that blanking for longer periods of time results in increasingly lower critical doses further corroborates this hypothesis, as the longer blanking intervals give the reacting species more time to diffuse and thus, to cause more damage. We expect that at beam blanking times on the order of nanoseconds (the time it would take for a radical to diffuse ~1 nm),[46] beam blanking would no longer change the critical dose, but we are unable to do this experiment due to technical limitations.

Additionally, an advantage of using conjugated polymers to study damage is that we are able to observe chemical damage by looking at the decay of low-loss electron energy loss spectroscopy (EELS) peaks.[35] EELS critical dose experiments show the same trend as in diffraction experiments: as dose rate is increased, the critical dose also increases (**Figure S2**). This suggests that damage to the core is time-dependent, which would not be the case if side chains were just cross linking without prior rearrangement through diffusion of radicals. Although our EELS experiments were conducted at a lower accelerating voltage to increase low-loss signal, the trends observed at 80kV should be representative of damage behavior at higher accelerating

voltages because the scattering cross section scales linearly with the inverse of accelerating voltage.

Conclusions

In this work, we systematically characterized beam damage in a series of conjugated polymers by measuring the critical dose under various conditions. We find that at room temperature, the critical dose increases with increasing dose rate, decreases with longer side chains, and decreases with beam blanking in between measurements. We find that cryogenic conditions increase polymer stability under the electron beam by an order of magnitude. Using our optimized dose conditions taken from critical dose experiments, we were able to directly image the 3.6 Å π-π stacking with HRTEM in a solution-processed conjugated polymer. This work not only reveals that beam damage in conjugated polymers occurs through the diffusion of a reacting species, but also demonstrates that with careful minimization of beam damage, current instrumentation is capable of imaging beam sensitive materials such as solution-processed conjugated polymers at the molecular scale.

Supporting Information

Supporting information, including details on GIWAXS and EELS, is available at xxx.

Acknowledgements

The authors acknowledge financial support from NSF through Award DMR-1609417 and DMR-1905550. B.K. acknowledges support by the DOE Office of Science Graduate Fellowship program and the Advanced Light Source Doctoral Fellowship in Residence. Work at the Molecular

Foundry was supported by the Office of Science, Office of Basic Energy Sciences of the U.S. Department of Energy under contract no. DE-AC02-05CH11231. This research used resources of the Advanced Light Source, which is a DOE Office of Science User Facility under contract no. DE-AC02-05CH11231. The authors thank C. Song for assistance with EELS alignment on the TEAM 0.5.

References

1. Erni, R.; Rossell, M. D.; Kisielowski, C.; Dahmen, U., Atomic-resolution imaging with a sub-50-pm electron probe. *Phys Rev Lett* **2009,** *102* (9), 096101.

2. Glaeser, R. M., Limitations to Significant Information in Biological Electron Microscopy as a Result of Radiation Damage. *J. Ultrastructure Research* **1971,** *36*, 466-482.

3. Glaeser, R. M., Retrospective: Radiation damage and its associated "Information Limitations". *Journal of Structural Biology* **2008,** *163*, 271-276.

4. Kuei, B.; Aplan, M. P.; Litofsky, J. H.; Gomez, E. D., New opportunities in transmission electron microscopy of polymers. *Materials Science and Engineering: R: Reports* **2020,** *139*, 100516.

5. Martin, D. C.; Thomas, E. L., Experimental high-resolution electron microscopy of polymers. *Polymer* **1995,** *36* (9), 1743-1759.

6. Thomas, E. L., Transmission electron microscopy of polymers. *Conference on Electron Microscopy and Crystallography in Polymer Science* **1987**, 422-425.

7. Doerr, A., Single-particle cryo-electron microscopy. *Nature Methods* **2016,** *13* (1), 23.

8. Li, X.; Mooney, P.; Zheng, S.; Booth, C. R.; Braunfeld, M. B.; Gubbens, S.; Agard, D. A.; Cheng, Y., Electron counting and beam-induced motion correction enable near-atomic-resolution single-particle cryo-EM. *Nat Methods* **2013,** *10* (6), 584-90.

9. Scheres, S. H., RELION: implementation of a Bayesian approach to cryo-EM structure determination. *J Struct Biol* **2012,** *180* (3), 519-30.

10. Lowe, J.; Li, H.; Downing, K. H.; Nogales, E., Refined Structure of ab-Tubulin at 3.5 A Resolution. *J. Mol. Biol.* **2001,** *313*, 1045-1057.

11. Bartesaghi, A.; Merk, A.; Banerjee, S.; Matthies, D.; Wu, X.; Milne, J. L. S.; Subramaniam, S., 2.2 A resolution cryo-EM structure of B-galactosidase in complex with a cell-permeant inhibitor. *Science* **2015,** *348*, 1147-1151.

12. Jiang, X.; Greer, D. R.; Kundu, J.; Ophus, C.; Minor, A. M.; Prendergast, D.; Zuckermann, R. N.; Balsara, N. P.; Downing, K. H., Imaging Unstained Synthetic Polymer Crystals and Defects on Atomic Length Scales Using Cryogenic Electron Microscopy. *Macromolecules* **2018,** *51* (19), 7794-7799.

13. Martin, D. C.; Thomas, E. L., Ultrastructure of poly(p-phenylenebenzobisoxazole) fibers. *Macromolecules* **1991,** *24*, 2040-2460.

14. Masse, M. A.; Martin, D. C.; Thomas, E. L.; Karasz, F. E.; Petermann, J. H., Crystal morphology in pristine and doped films of poly (p-phenylene vinylene). *Journal of Materials Science* **1990,** *25*, 311-320.

15. Miller, A. A., Effects of high-energy radiation on polymers. *Annals of the New York Academy of Sciences* **1959**.

16. Grubb, D. T., Radiation damage and electron microscopy of organic polymers. *Journal of Materials Science* **1974,** *9*, 1715-1736.

17. Chapiro, A., *Radiation Chemistry of Polymeric Systems*. John Wiley & Sons: New York, 1962.

18. Drummy, L. F.; Davis, R. J.; Moore, D. L.; Durstock, M.; Vaia, R. A.; Hsu, J. W. P., Molecular-Scale and Nanoscale Morphology of P3HT:PCBM Bulk Heterojunctions: Energy-Filtered TEM and Low-Dose HREM†. *Chem. Mater.* **2011,** *23* (3), 907-912.

19. Takacs, C. J.; Treat, N. D.; Kramer, S.; Chen, Z.; Facchetti, A.; Chabinyc, M. L.; Heeger, A. J., Remarkable order of a high-performance polymer. *Nano Lett* **2013,** *13* (6), 2522-7.

20. O'Hara, K.; Takacs, C. J.; Liu, S.; Cruciani, F.; Beaujuge, P.; Hawker, C. J.; Chabinyc, M. L., Effect of Alkyl Side Chains on Intercrystallite Ordering in Semiconducting Polymers. *Macromolecules* **2019,** *52* (7), 2853-2862.

21. Noriega, R.; Rivnay, J.; Vandewal, K.; Koch, F. P. V.; Stingelin, N.; Smith, P.; Toney, M. F.; Salleo, A., A general relationship between disorder, aggregation and charge transport in conjugated polymers. *Nat. Mater.* **2013,** *12* (11), 1037-1043.

22. Kline, J. R.; McGehee, M. D.; Toney, M. F., Highly oriented crystals at the buried interface in polythiophene thin-film transistors. *Nat. Mater.* **2006,** *5*, 222.

23. Vakhshouri, K.; Smith, B. H.; Chan, E. P.; Wang, C.; Salleo, A.; Wang, C.; Hexemer, A.; Gomez, E. D., Signatures of Intracrystallite and Intercrystallite Limitations of Charge Transport in Polythiophenes. *Macromolecules* **2016,** *49* (19), 7359-7369.

24. Yang, H.; Shin, T. J.; Yang, L.; Cho, K.; Ryu, C. Y.; Bao, Z., Effect of Mesoscale Crystalline Structure on the Field-Effect Mobility of Regioregular Poly(3-hexyl thiophene) in Thin-Film Transistors. *Adv. Funct. Mater.* **2005,** *15* (4), 671-676.

25. Sirringhaus, H.; Brown, P. J.; Friend, R. H.; Nielsen, M. M.; Bechgaard, K.; Langeveld-Voss, B. M. W.; Spiering, A. J. H.; Janssen, R. A. J.; Meijer, E. W.; Herwig, P.; de

Leeuw, D. M., Two-dimensional charge transport in self-organized, high-mobility conjugated polymers. *Nature* **1999,** *401* (6754), 685-688.

26. Thomas, D. C. M. a. E. L., Experimental high-resolution electron microscopy of polymers. *Polymer* **1995,** *36* (9), 1743-1759.

27. Russo, C. J.; Egerton, R. F., Damage in electron cryomicroscopy: Lessons from biology for materials science. *MRS Bulletin* **2019,** *44*, 935-941.

28. Martin, D. C.; Chen, J. H.; Yang, J. Y.; Drummy, L. F.; Kubel, C., High resolution electron microscopy of ordered polymers and organic molecular crystals: Recent developments and future possibilities. *Journal of Polymer Science Part B-Polymer Physics* **2005,** *43* (14), 1749-1778.

29. Roehling, J. D.; Baran, D.; Sit, J.; Kassar, T.; Ameri, T.; Unruh, T.; Brabec, C. J.; Moulé, A. J., Nanoscale Morphology of PTB7 Based Organic Photovoltaics as a Function of Fullerene Size. *Sci. Rep.* **2016,** *6* (1), 30915.

30. Libera, K. S. a. M., The influence of fast secondary electrons on the aromatic structure of polystyrene. *Philosophical Magazine A* **2000,** *80* (4), 1001-1016.

31. Egerton, R. F.; Rauf, I., Dose-rate dependence of electron-induced mass loss from organic specimens. *Ultramicroscopy* **1999,** *80*, 247-254.

32. Leijten, Z. J. W. A.; Keizer, A. D. A.; With, G. d.; Friedrich, H., Quantitative Analysis of Electron Beam Damage in Organic Thin Films. *J. Phys. Chem. C* **2017,** *121*, 10552-10561.

33. Read, R. T.; Young, R. J., Radiation damage and high resolution electron microscopy of polydiacetylene crystals. *Journal of Materials Science* **1984,** *19*, 327-338.

34. Warkentin, M.; Hopkins, J. B.; Badeau, R.; Mulichak, A. M.; Keefe, L. J.; Thorne, R. E., Global radiation damage: temperature dependence, time dependence and how to outrun it. *J. Synchrotron Rad.* **2012,** *20*, 7-13.

35. Guo, C.; Allen, F.; Lee, Y.; Le, T. P.; Song, C.; Ciston, J.; Minor, A. M.; Gomez, E. D., Probing Local Electronic Transitions in Organic Semiconductors through Energy-Loss Spectrum Imaging in the Transmission Electron Microscope. *Adv. Funct. Mater.* **2015,** *25*, 6071-6076.

36. Leijten, Z.; Keizer, A. D. A.; de With, G.; Friedrich, H., Quantitative Analysis of Electron Beam Damage in Organic Thin Films. *J Phys Chem C Nanomater Interfaces* **2017,** *121* (19), 10552-10561.

37. Liu, Y.; Zhao, J.; Li, Z.; Mu, C.; Ma, W.; Hu, H.; Jiang, K.; Lin, H.; Ade, H.; Yan, H., Aggregation and morphology control enables multiple cases of high-efficiency polymer solar cells. *Nature Communications* **2014,** *5*, 5293.

38. Ma, W.; Yang, G.; Jiang, K.; Carpenter, J. H.; Wu, Y.; Meng, X.; McAfee, T.; Zhao, J.; Zhu, C.; Wang, C.; Ade, H.; Yan, H., Infl uence of Processing Parameters and Molecular Weight on the Morphology and Properties of High-Performance PffBT4T-2OD:PC 71 BM Organic Solar Cells *Adv. Energy Mater.* **2015**, 1501400.

39. Panova, O.; Ophus, C.; Takacs, C. J.; Bustillo, K. C.; Balhorn, L.; Salleo, A.; Balsara, N.; Minor, A. M., Diffraction imaging of nanocrystalline structures in organic semiconductor molecular thin films. *Nat. Mater.* **2019,** *18* (8), 860-865.

40. Kuei, B.; Gomez, E. D., Pushing the limits of high-resolution polymer microscopy using antioxidants. *Submitted* **2020**.

41. Miller, A. A., Effects of high-energy radiation on polymers. *Annals of the New York Academcy of Sciences* **1959**.

42. Mund, W.; Bogaert, E., *Bull. soc. chim. Belges* **1925,** *34* (410).

43. Miller, A. A., Effects of high-energy radiation on polymers. *Ann. NY. Acad. Sci.* **1959**, 774-781.

44. Jaworska, E.; Kaluska, I.; Strzelczak-Burlinska, G.; Michaelik, J., Irradiation of polyethylene in the presence of antioxidants. *Radiat. Phys. Chem.* **1991,** *37* (2).

45. van Bavel, S. S.; Loos, J., Volume Organization of Polymer and Hybrid Solar Cells as Revealed by Electron Tomography. *Adv. Funct. Mater.* **2010,** *20* (19), 3217-3234.

46. Kuei, B.; Aplan, M. P.; Litofsky, J. H.; Gomez, E. D., New opportunities in transmission electron microscopy of polymers. *Materials Science and Engineering: R: Reports* **2020,** *139*.